

EXPERIMENTAL INVESTIGATION OF BLOWING RATIO EFFECT ON FLOW REGIMES OF TRANSPIRATION COOLING IN LATTICE POROUS MEDIA

Jaeseung Heo[1], Jinung Lee[1], Reynolds Addo-Akoto[1], Jaehan Cho[1,2] & Jae-Hung Han[1]

[1]Department of Aerospace Engineering, Korea Advanced Institute of Science and Technology, Daejeon 34131, Korea
[2]Agency for Defense Development, Yuseong, Daejeon 34186, Korea

Abstract

Transpiration cooling is an effective active cooling approach for high heat flux environments, offering high cooling efficiency with low coolant consumption. During operation, a liquid coolant absorbs heat as it evaporates within a porous medium, forming a cooling layer at the heated surface. However, conventional porous media often exhibit vapor-induced flow instability and non-uniform cooling because their pore network is randomly distributed and cannot be controlled at the pore scale. Additive manufacturing (AM) overcomes these limitations by enabling precise control of the porous internal geometry. In this study, an octa-radial of the simple cubic body-centered cubic (SC-BCC) lattice is fabricated by stereolithography (SLA). The transpiration cooling performance is experimentally investigated in an open hot-air wind tunnel at four blowing ratios F, defined as the ratio of coolant to mainstream mass flux, of 0.17%, 0.22%, 0.28%, and 0.33% under phase-change conditions. Three distinct flow regimes are identified, namely dry-out (F = 0.22% and 0.17%), phase-change (F = 0.28%), and partial phase-change (F = 0.33%), with the cooling efficiency increasing from 71% to 92% as the blowing ratio increases. The phase-change regime at F = 0.28% provides the most favorable combination of cooling efficiency, peak local surface temperature, and spatial uniformity without flow instability, identifying it as the optimal operating window for the present lattice configuration.

Keywords: Transpiration Cooling, Porous Media, Lattice Structures, Phase Change

1. Introduction

Reusable spacecraft and high-speed flight vehicles are exposed to severe aerodynamic heating during atmospheric flights, where intense thermal loads are concentrated over critical surface regions [1]. To address these extreme thermal environments, active cooling systems have emerged as a promising thermal protection system (TPS) for applications subjected to sustained high heat fluxes [2]. Transpiration cooling, in which the coolant flows outward through a porous wall and absorbs heat on its way to the heated surface, offers high cooling efficiency with low coolant consumption compared to other active methods [3]. In particular, deionized water-based transpiration cooling provides superior performance compared to gas-based systems due to the high specific heat capacity and latent heat of vaporization of water [4]. Among water-based approaches, phase change transpiration cooling has attracted strong interest because the coolant evaporation further enhances the achievable heat removal rate at the heated surface [5].

Previous transpiration cooling studies have mainly focused on sintered porous materials and composites. However, these conventional porous materials often exhibit cooling non-uniformity caused by random microstructures and irregular internal flow paths, leading to localized cooling inefficiencies [5,6]. In sintered metals, the random pore distribution produces anisotropic permeability and localized overheating. Adjusting the coolant flow rate alone cannot achieve a spatially uniform

temperature field, because the underlying pore network is itself non-uniform. Recent advances in additive manufacturing (AM) have made it feasible to fabricate aerospace components with reliable feature reproducibility and tight pore-scale dimensional control [7,8]. This capability allows improved control of internal flow paths in transpiration cooling applications, helping to mitigate non-uniform coolant distribution and localized cooling inefficiencies associated with conventional sintered porous media [8].

Strut-based lattices are used in AM-based porous structures because their porosity, permeability, and fluid–solid contact area can be tuned independently through the strut diameter, length, and connectivity [9]. This independent control distinguishes them from sintered porous media, where these parameters are coupled. Among strut-based lattices, the simple cubic body-centered cubic (SC-BCC) configuration stands out for its favorable balance of structural rigidity and thermohydraulic performance. Its systematic cell arrangement forms uniform pore networks that promote consistent coolant flow and provide large heat-transfer surface area while keeping the pressure drop moderate, making the SC-BCC structure a suitable reference geometry for transpiration cooling studies [10]. Among the SC-BCC variants, the octa-radial configuration connects every corner node of the simple cubic (SC) cell to the centered body-centered cubic (BCC) node, forming a point-symmetric eight-leg pore network (see Fig. 1). The octa-radial configuration is selected in this study as the representative SC-BCC variant for examining cooling behavior in AM-based lattice porous media.

Previous studies [8, 11] have demonstrated the feasibility of transpiration cooling using additively manufactured porous structures. Shin et al. [12] classified phase-change transpiration cooling in sintered porous media into four flow regimes (all-liquid, partial phase-change, phase-change, and dry-out) according to coolant flow rate, but the corresponding classification has not been reported for AM-based lattice porous media. Since the blowing ratio governs these transitions, its effect on the temporal evolution of the liquid–vapor distribution and the resulting surface-temperature uniformity must be characterized. In this study, an additively manufactured octa-radial SC-BCC lattice is experimentally investigated in an open hot-air wind tunnel under varying blowing ratio. Surface temperature distributions are evaluated using transient temperature measurements and infrared thermography to assess both temporal and spatial cooling uniformity. The resulting flow regimes are classified by their temporal variation, peak surface temperature, and flow stability. This identifies the operating range that achieves uniform cooling without flow instability.

2. Experimental Setup

2.1 Porous media design and manufacturing

Figure 1 illustrates the additively manufactured porous specimen investigated in this study. The specimen has an overall thickness of 8 mm, and its lattice region covers an area of 30 mm × 30 mm with 900 octa-radial lattice structure unit cells arranged in a 15 × 15 × 4 array. This regular internal structure supports systematic investigation of coolant flow and cooling performance in AM-based lattice porous media [11].

The unit cell length was set to 2 mm, the minimum cell size at which the SLA printer can reliably resolve the lattice features without internal blockage. The porosity was maintained at approximately 50% by setting the fin diameter to d_{fin} = 0.628 mm. This porosity level was selected to ensure reliable fabrication within the resolution limits of the SLA process while preserving the structural integrity of the porous specimen.

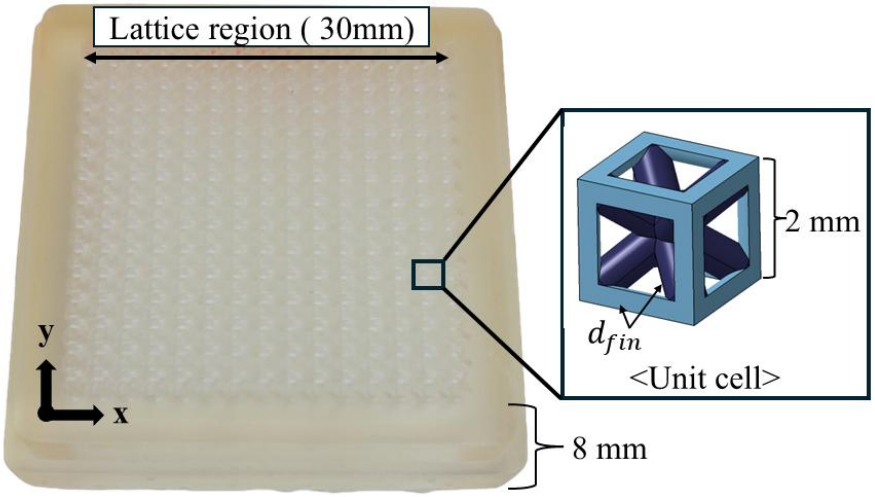


Figure 1 – Additively manufactured porous specimen and octa-radial lattice structure unit cell geometry.

The permeability of the lattice region was measured from a separate flow-rate–pressure-drop test. Deionized water was supplied through the specimen at controlled volumetric flow rates, and the corresponding pressure drop across the lattice region was monitored. The permeability *K* was then obtained from the measured flow rate and pressure drop using Darcy's law, as given in Eq. (1).

$$K = \frac{Q\,\mu_f\,t}{A\,\Delta P} \qquad (1)$$

Here, Q is the volumetric flow rate, μ_f is the dynamic viscosity of the working fluid, t is the specimen thickness (8 mm), A is the cross-sectional area of the lattice region (900 mm^2), and ΔP is the measured pressure drop. The coolant was supplied at five mass flow rates of approximately 1.66 × 10^{-5}, 8.31 × 10^{-5}, 1.66 × 10^{-4} , 4.99 × 10^{-4} , and 8.31 × 10^{-4} kg/s and the pressure drop across the lattice region was measured at each set point. The pressure drop varied linearly with the flow rate over this range, indicating that the flow remained in the laminar Darcy regime. The measured permeability was K = 2.11 × 10^{-9} m².

The porous specimen was fabricated using a stereolithography (SLA) 3D printer (Formlabs, Form 3+), with High Temp Resin (Formlabs) selected as the fabrication material. The unit cell dimensions were designed based on the minimum printable feature size supported by the SLA printer. The fabrication process involved printing, cleaning, and curing. After printing, the specimen was ultrasonically cleaned in isopropyl alcohol for 10 minutes, repeated twice, to remove uncured resin from the internal lattice cavities and preserve the as-designed feature resolution. The specimen was then post-cured at 353 K for 130 minutes to enhance mechanical strength.

2.2 Experimental apparatus

The transpiration cooling experiments were conducted in an open hot-air wind tunnel. Figure 2 shows a schematic of the overall test apparatus, consisting of the mainstream supply line, the test section, and the coolant supply line. In the mainstream supply line, atmospheric air was supplied by a ring blower (KJB3-750, Inha Glotech), passed through a filter and a control valve, and heated by a 10 kW electric heater (Super Air Heater, Gookmin Heater) regulated by a temperature controller (VX7, Gookmin Heater). The heated mainstream air was then discharged into the open test section through a rectangular outlet with a cross-sectional area of 40 mm × 40 mm. The mainstream temperature was maintained at approximately 670 K, and the freestream velocity was set to 11 m/s, corresponding to a Reynolds number of approximately 1.2 × 10^4 based on the porous specimen length. In the coolant supply line, deionized water was supplied to the porous specimen at controlled mass flow rates by a two-head piston pump (UI-22, FLOM) and a mass flow meter (LF3000, Siargo). Surface temperature distributions were measured using an infrared camera (A50, Teledyne FLIR), and K-type thermocouples (KMQXL-062U-6, Omega Engineering) were used to monitor the coolant and chamber temperatures.

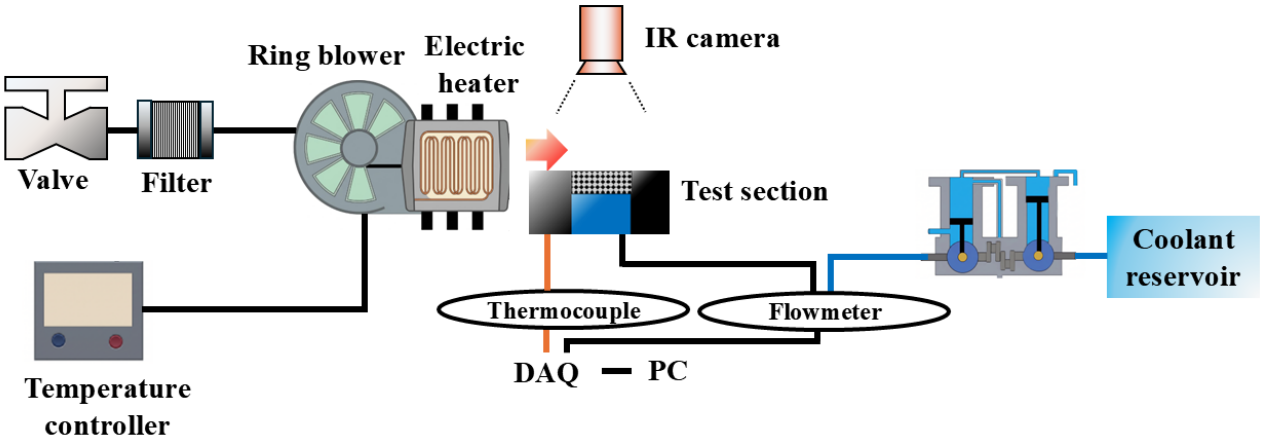


Figure 2 – Schematic of the experimental apparatus for the transpiration cooling experiments.

The coolant supply was characterized using the dimensionless blowing ratio, defined as

$$F = \frac{\rho_c u_c}{\rho_\infty u_\infty} \qquad (2)$$

where ρ_c and u_c are the density and velocity of the coolant, and ρ_∞ and u_∞ are those of the mainstream.

To characterize the spatial uniformity of the surface temperature, the local surface temperature distribution within the lattice region is analyzed at each characteristic time point. The maximum and minimum local surface temperatures, $T_{w,max}$ and $T_{w,min}$ are extracted directly from the IR image. The spatial standard deviation σ_T, which quantifies the overall non-uniformity of the temperature distribution, is defined as

$$\sigma_T = \sqrt{\frac{1}{N}\sum_{x,y}\left(T_w(x,y) - \overline{T}_w\right)^2} \qquad (3)$$

where $T_w(x,y)$ is the local surface temperature at pixel (x, y) of the lattice region, $\overline{T}_w$ is the spatially averaged surface temperature, and N is the number of pixels within the lattice region.

The overall cooling effectiveness is further characterized by the spatially and time-averaged cooling efficiency, defined as

$$\overline{\eta} = \frac{T_\infty - \overline{T}_w}{T_\infty - T_c} \qquad (4)$$

where T_∞ is the mainstream temperature, $\overline{T}_w$ is the spatially averaged surface temperature of the lattice region, and T_c is the coolant temperature. Throughout the present work, the reported $\overline{\eta}$ values are further time-averaged over the 0–300 s measurement interval.

3. Experimental Procedure and Results

3.1 Experimental procedure

For each test condition, the coolant supply was first stabilized at F = 0.56% for 420 s to prevent unintended boiling, then transitioned over 30 s to the target mass flux while the mainstream remained constant. Temperature and flow data were then recorded for 300 s at four blowing ratios of F = 0.17%, 0.22%, 0.28%, and 0.33% (corresponding to G = 0.017, 0.022, 0.028, and 0.033 kg/m²s, respectively, where $G = \rho_c u_c$).

3.2 Flow regime characterization

Figure 3 presents the time histories of the spatially averaged surface temperature $\overline{T}_w$ and representative IR images of the lattice region from F = 0.17% to 0.33%. Four characteristic time points, labeled (A)–(D) on Fig. 3 (left),have their corresponding IR images shown in the figures on the right. Three distinct flow regimes are identified, namely partial phase-change (F = 0.33%), phase-change (F = 0.28%), and dry-out (F = 0.22% and 0.17%). Each regime is described below in terms of its transient temperature response and the underlying liquid–vapor transport mechanism within the

porous medium, with the latter schematically shown in Fig. 4.

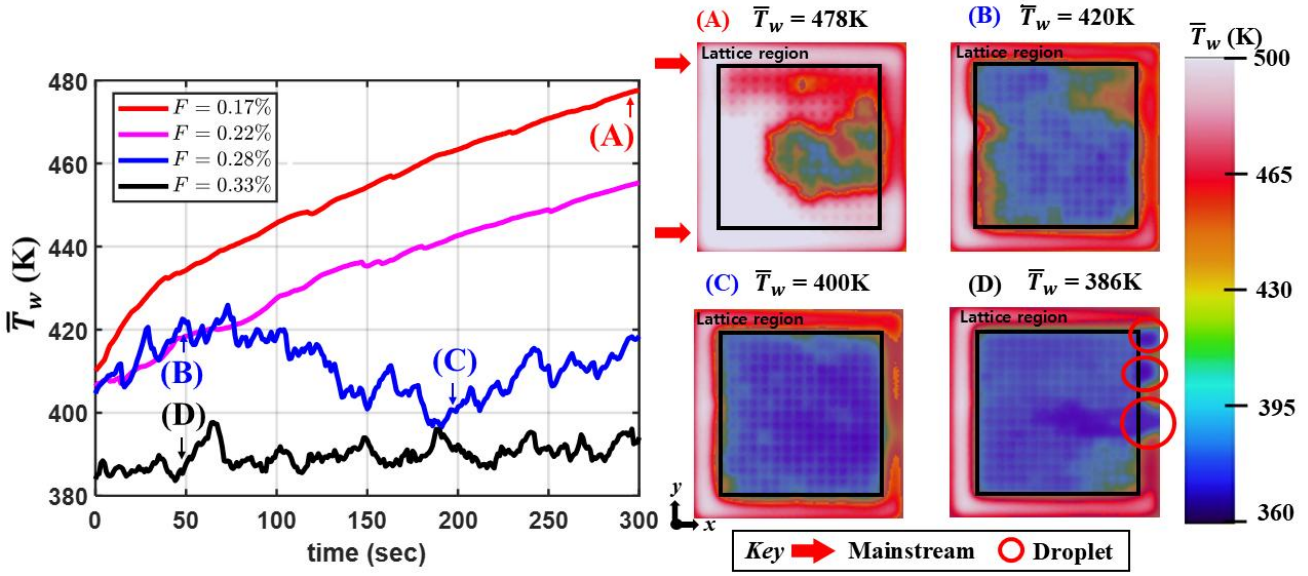


Figure 3 – Cooling characteristics in the octa-radial lattice (K = 2.11 × 10⁻⁹ m²): (left) time histories of $\overline{T}_w$ and (right) IR images at characteristic time points

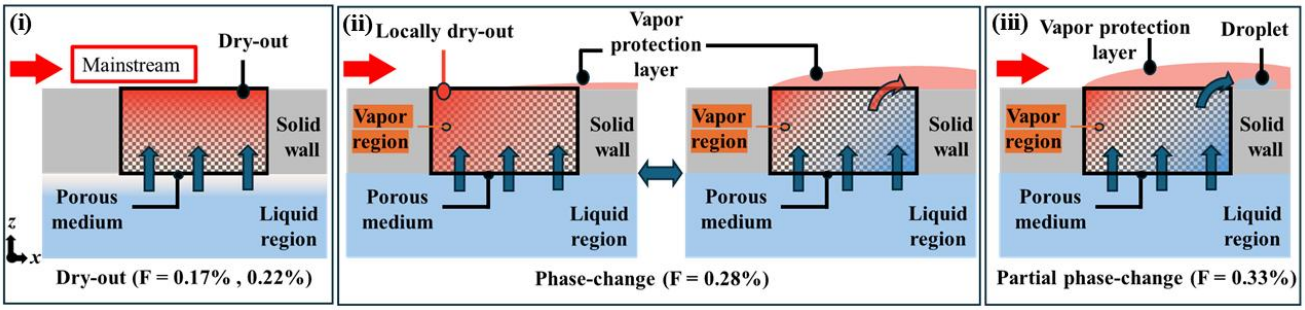


Figure 4 – Cross-section schematics of internal liquid–vapor distribution mechanisms in the octa-radial lattice structure (K = 2.11 × 10⁻⁹ m²) for the three flow regimes

3.2.1 Dry-out flow regime (F = 0.22% and 0.17%)

In the dry-out regime, observed at both F = 0.22% and F = 0.17%, $\overline{T}_w$ increased monotonically throughout the 300 s measurement period with no cooling recovery. The rise was most severe at F = 0.17%, where $\overline{T}_w$ climbed to a peak of approximately 479 K, while at F = 0.22% the heating was more gradual, peaking near 457 K. The corresponding Fig. 3(A) at F = 0.17% reveals a severely overheated and non-uniformly wetted lattice surface with extensive hot spots, indicating that the supplied coolant flow rate was insufficient to overcome the imposed external heat load. As schematically illustrated in Fig. 4(i), an expanded vapor region accumulated in the upper portion of the porous medium and blocked liquid penetration from below, preventing the formation of a sustained vapor protection layer above the lattice surface. The lattice surface progressively dried out and was exposed to direct contact with the high-temperature mainstream. This regime constitutes a hazardous operating condition that may cause structural damage and must be strictly avoided in transpiration cooling system design.

3.2.2 Phase-change flow regime (F = 0.28%)

At F = 0.28%, $\overline{T}_w$ exhibited a repeated pattern of temporary rise followed by gradual cooling, with the temperature confined to a narrow range of approximately 23 K throughout the 300 s measurement period. As illustrated by Fig. 3(B) and (C), the lattice region alternated between a brief localized heating phase and a uniform cooling phase, with no droplet ejection or persistent local overheating throughout the cycle. Figure 4(ii) schematically depicts the underlying mechanism, in which the vapor protection layer above the lattice surface alternated between a locally dry-out state and a regrowth state, driven by continuous coolant resupply through the uniform pore network of the octa-radial lattice structure. The surface temperature therefore remained well below the structural integrity limit of the

lattice material throughout the measurement period. The intermittent rewetting of this cycle effectively utilizes the latent heat of vaporization. Coolant consumption is therefore reduced while cooling performance is maintained. Among the three flow regimes tested, this regime combined a narrow temporal range, a uniform spatial distribution, and a low peak surface temperature without flow instability. This combination represents the most attractive operating point when both temperature uniformity and stable operation are required.

3.2.3 Partial phase-change flow regime (F = 0.33%)

At the highest blowing ratio of F = 0.33%, $\overline{T}_w$ exhibited mild temporal fluctuations within a range of approximately 9 K. The corresponding Fig. 3(D) shows a slightly non-uniform temperature distribution with intermittent droplet ejection from the lattice surface. As schematically illustrated in Fig. 4(iii), vapor formed only partially at the top of the porous medium, with a thin vapor protection layer through which droplets were ejected. In this partially two-phase state, the viscosity contrast between liquid water and steam, by a factor of approximately 15–20, produced local pressure-drop variations that drove the droplet ejection and the onset of flow instability. Although the surface remained predominantly wetted by the coolant, the latent heat utilization was limited because phase change occurred over only a fraction of the surface. The persistent droplet ejection therefore reflects an unfavorable mode of excessive coolant consumption.

3.3 Spatial temperature uniformity

To characterize the spatial uniformity of the surface temperature in each flow regime, the local surface temperature distribution within the lattice region was extracted from the IR images at the four characteristic time points (A)–(D) shown in Fig. 3. The resulting maximum, minimum, and spatial standard deviation values are summarized in Table 1.

Table 1 – Minimum and maximum local surface temperature calculated from the IR images for F = 0.17% to 0.33%.

F (%)	Flow regime	$T_{w,max}$ (K)	$T_{w,min}$ (K)	σ_T (K)
0.17	Dry-out	532.1	411.2	34.2
0.28	Phase-change (localized heating)	492.3	397.6	18.0
0.28	Phase-change (uniform cooling)	453.0	386.4	9.4
0.33	Partial phase-change	426.9	366.5	7.9

The maximum local surface temperature $T_{w,max}$and the spatial standard deviation $\sigma_T$both decreased monotonically with increasing blowing ratio. The dry-out condition at F = 0.17%, shown in Fig. 3(A), exhibited the largest values, with $T_{w,max}$ = 532.1 K and σ_T = 34.2 K, reflecting the extensive hot spots characteristic of the dry-out regime. The phase-change condition at F = 0.28% reduced these values to $T_{w,max}$ = 492.3 K and σ_T = 18.0 K during the localized heating phase shown in Fig. 3(B), and further to $T_{w,max}$ = 453.0 K and σ_T = 9.4 K during the subsequent uniform cooling phase shown in Fig. 3(C). At F = 0.33%, shown in Fig. 3(D), the partial phase-change regime exhibited the smallest values of $T_{w,max}$ = 426.9 K and σ_T = 7.9 K, although the lattice was simultaneously disturbed by intermittent droplet ejection.

These results demonstrate that the spatial uniformity improved dramatically across the regime transition from dry-out to phase-change. The phase-change regime at F = 0.28% maintained σ_T below 18.0 K even at its worst-case localized heating phase, approximately half of the dry-out value, and dropped to 9.4 K during its uniform cooling phase, only 1.5 K above the smallest value observed in the partial phase-change regime. Although the partial phase-change regime achieved a marginally smallest σ_T, the persistent droplet ejection rendered it unsuitable for stable operation, making the phase-change regime the more attractive operating point overall.

3.4 Cooling efficiency

The cooling efficiency $\overline{\eta}$ provides an overall measure of the cooling performance, complementing the spatial uniformity descriptors. Figure 5 plots $\overline{\eta}$ as a function of the blowing ratio F. The cooling efficiency increased monotonically with F, rising from 71.3% at F = 0.17% to 80.9% at F = 0.22%, 87.6% at F = 0.28%, and 92.2% at F = 0.33%. The increment between successive blowing ratios, however, decreased monotonically from 9.6 percentage points within the dry-out regime to 6.7 percentage points across the dry-out-to-phase-change transition and to 4.6 percentage points across the phase-change-to-partial-phase-change transition. This diminishing rate of improvement at higher blowing ratios reflects the asymptotic approach of $\overline{\eta}$ to its theoretical maximum of unity, attained when the spatially averaged surface temperature equals the coolant inlet temperature.

Although the partial phase-change regime at F = 0.33% exhibited the highest cooling efficiency, the persistent droplet ejection associated with the partial two-phase state rendered it an unstable operating condition. The phase-change regime at F = 0.28% therefore provided a more attractive operating point, combining a sufficiently high cooling efficiency with the spatial uniformity and stability documented in Table 1.

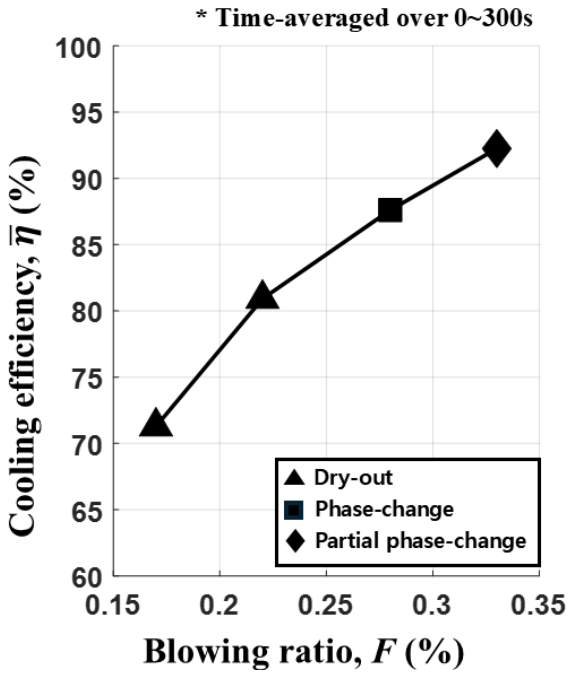


Figure 5 – Cooling efficiency $\overline{\eta}$ of the octa-radial SC-BCC lattice structure (K = 2.11 × 10⁻⁹ m²) as a function of blowing ratio F.

4 Conclusion

In this study, the transpiration cooling characteristics of an additively manufactured octa-radial SC-BCC lattice structure (K = 2.11 × 10⁻⁹ m²) were experimentally investigated under external hot-air flow at four blowing ratios of F = 0.17%, 0.22%, 0.28%, and 0.33%. Three distinct flow regimes were identified, namely dry-out (F = 0.22% and 0.17%), phase-change (F = 0.28%), and partial phase-change (F = 0.33%). Each regime is characterized by a distinct transient temperature response and a distinct liquid–vapor transport mechanism within the lattice porous medium. The cooling efficiency $\overline{\eta}$ increased monotonically with the blowing ratio, from 71.3% at F = 0.17% to 92.2% at F = 0.33%, while the peak local surface temperature $T_{w,max}$ decreased from 532.1 K to 426.9 K. The spatial standard deviation σ_T showed the most pronounced improvement across the regime transition, dropping from 34.2 K in the dry-out regime to less than 10 K in the phase-change and partial phase-change regimes. Although the partial phase-change regime exhibited the highest cooling efficiency and the smallest spatial standard deviation, the persistent droplet ejection rendered it an unstable operating condition. The phase-change regime at F = 0.28% therefore provided the most favorable operating point, combining a sufficiently high cooling efficiency, a moderate peak surface temperature, and a uniform spatial distribution without flow instability. These findings demonstrate the existence of an optimal blowing ratio and provide practical guidance for the design and operation of additively

manufactured octa-radial lattice structures for transpiration cooling.

5 Acknowledgements

This work is supported by Korea Research Institute for Defense Technology Planning and Advancement (KRIT) grant funded by the Korea Government (DAPA (Defense Acquisition Program Administration)) (No. KRIT-CT-22-030, Reusable Unmanned Space Vehicle Research Center, 2026). This work is also supported by the Agency for Defense Development.

6 Contact Author Email Address

Jaeseung Heo: tlsdkawotmd@kaist.ac.kr

Jinung Lee: wlsdnd5309@kaist.ac.kr

Reynolds Addo-Akoto: reykoto@kaist.ac.kr

Jaehan Cho: jaehancho@kaist.ac.kr

Jae-Hung Han (Corr. Author): jaehunghan@kaist.ac.kr

7 Copyright Statement

The authors confirm that they, and/or their company or organization, hold copyright on all of the original material included in this paper. The authors also confirm that they have obtained permission, from the copyright holder of any third party material included in this paper, to publish it as part of their paper. The authors confirm that they give permission, or have obtained permission from the copyright holder of this paper, for the publication and distribution of this paper as part of the ICAS proceedings or as individual off-prints from the proceedings.

References

[1] Park Y and Shin E S. Thermal-structural coupled analysis and design of a reentry capsule with ablative thermal protection systems. *International Journal of Aeronautical and Space Sciences*, Vol. 26, No. 4, pp 1534-1546, 2025.

[2] Uyanna O and Najafi H. Thermal protection systems for space vehicles: A review on technology development, current challenges and future prospects. *Acta Astronautica*, Vol. 176, pp 341-356, 2020.

[3] Mi Q, Yi S H, Gang D D, Lu X G and Liu X L. Research progress of transpiration cooling for aircraft thermal protection. *Applied Thermal Engineering*, Vol. 236, pp 121360, 2024.

[4] Wang J, Zhao L, Wang X, Ma J and Lin J. An experimental investigation on transpiration cooling of wedge-shaped nose cone with liquid coolant. *International Journal of Heat and Mass Transfer*, Vol. 75, pp 442-449, 2014.

[5] He F, Wang J, Xu L and Wang X. Modeling and simulation of transpiration cooling with phase change. *Applied Thermal Engineering*, Vol. 58, No. 1-2, pp 173-180, 2013.

[6] Li X, Liao Z, Li H, Jiang P and Xu R. Phase-change transpiration cooling in heterogeneous composite porous plates: Heat transfer characteristics and their prediction. *International Journal of Heat and Mass Transfer*, Vol. 224, pp 125290, 2024.

[7] Che X, Xin R and Goo N S. Experimental and numerical study on 3D printed carbon fiber composite cylindrical shell under axial loading. *International Journal of Aeronautical and Space Sciences*, Vol. 26, No. 5, pp 2309-2329, 2025.

[8] Sheng Y, Wang J, Liu C and Wu N. Experimental study on transpiration cooling with additively manufactured porous structures. *Applied Thermal Engineering*, Vol. 213, pp 118710, 2022.

[9] Dixit T, Nithiarasu P and Kumar S. Numerical evaluation of additively manufactured lattice architectures for heat sink applications. International Journal of Thermal Sciences, Vol. 159, pp 106607, 2021.

[10] Jeong J-H, Heo J, Lee S, Kim S J and Han J-H. Numerical prediction of permeability and effective thermal conductivity in simple cubic and body-centered truss structures. *Journal of Fluids Engineering*, Vol. 147, No. 9, pp 091502, 2025.

[11] Heo J, Cho J, Addo-Akoto R, Lee J, Kim S J and Han J-H. Experimental investigation into the effect of coolant temperature on transpiration cooling in lattice structures. *Journal of Mechanical Science and Technology*, Vol. 40, No. 2, pp 1445-1457, 2026.

[12] Shin J, Bae J, Kim S J and Kim T Y. Flow regimes and flow instability of transpiration cooling.

International Journal of Heat and Mass Transfer, Vol. 252, pp 127457, 2025.